Nonlinear Coupling of Lower Hybrid Grills and Comparison with Experimental Data from ASDEX

V. Petrzilka*, F. Leuterer

IPP

IPP 4/243 September 1990

MAX-PLANCK-INSTITUT FÜR PLASMAPHYSIK

8046 GARCHING BEI MÜNCHEN

MAX-PLANCK-INSTITUT FÜR PLASMAPHYSIK
GARCHING BEI MÜNCHEN

Nonlinear Coupling of Lower Hybrid Grills and
Comparison with Experimental Data from ASDEX

V. Petrzilka*, F. Leuterer
IPP

IPP 4/243 September 1990

Abstract

In this paper, computations of the reflection coefficient based on the nonlinear lower hybrid (LH) coupling theory are presented and compared with measurements of the reflection coefficient of the ASDEX tokamak LH grill, where powers of up to 4 kW/cm^2 have been launched. Such a LH power density modifies the electron density in front of the grill as a result of ponderomotive forces. This changes the coupling and the power reflection coefficient R. Comparison of computed reflection coefficients with experimentally observed ones suggests that heating of the plasma in front of the grill by the transmitted LH power has also to be taken into account in order to explain the observed saturation of the growth of the reflection coefficient with power.

* Czechoslovak Academy of Sciences,
Institute of Plasma Physics, CS 18 211 Prague

Die nachstehende Arbeit wurde im Rahmen des Vertrages zwischen dem Max-Planck-Institut für Plasmaphysik und der Europäischen Atomgemeinschaft über die Zusammenarbeit auf dem Gebiete der Plasmaphysik durchgeführt.

1. Experimental power dependence of the reflection coefficient in ASDEX

A lower hybrid system with the frequency f = 2.45 GHz is in operation on the ASDEX tokamak / 1 /. The LH grill consists of two arrays of 24 waveguides each, arranged one on top of the other. The inner dimensions of the guides are 10 X 109 mm, with 4 mm walls in between. The vertical separation between the centers of the two grills is 160 mm. A phasing of $\Delta\varphi = 180°$ generates a symmetric spectrum with $N_{||} = 4.4$. The phase in each waveguide can be set arbitrarily with a corresponding shift in $N_{||}$, leading to asymmetric spectra used for current drive, such as $\Delta\varphi = 90°$ with $N_{||} = 2.2$. More details on the coupling with this grill can be found in /2/. Here we focus our attention on the power dependence of the average reflection coefficient.

In a first experimental campaign the grill was surrounded by graphite tiles which protruded 3 mm beyond the waveguides. In these conditions the average reflection coefficient R, at medium power levels, was between 20 % and 40 %, depending on the phasing. Such high reflection coefficients can be understood only if a layer of very low density in front of the waveguides is assumed. In linear coupling codes this situation can be modeled by introducing a vacuum gap of up to 2 mm between the grill and the plasma, yielding reasonable agreement / 2 /. However, there is also a variation of R with power, as shown in fig. 1. After an initial increase, R tends to saturate at high power levels. This is observed for all phasings.

In a later experimental campaign the graphite tiles had been cut back to make them flush with the waveguides. This improved the coupling by a factor of more than two, as seen in fig. 2, consistently with the assumption of no vacuum gap between the grill and plasma in the linear coupling theory /2/. However, R is still found to increase appreciably with power, again to a saturated level. A detailed inspection of reflection coefficients in each indi-vidual waveguide indicates a decreasing electron density in front of the grill when the power is increased /2/.

Probe measurements and X-mode reflectometer measurements /3/ indicate that under standard operation conditions we have an edge electron density in front of the grill of $n_{edge} \approx 5 \times 10^{11}$ cm^{-3} and a density gradient of $\nabla n_e \approx 4 \times 10^{11}$ cm^{-4}. The edge temperature is estimated to be about 5 -10 eV.

2. Short outline of the theory

The theory /4,5/ assumes a very long grill in the poloidal (y) and toroidal (z) directions (see also /6,7,8/) and step and ramp profiles for the unperturbed plasma density n_0 and the plasma temperature T:

$$(1) \qquad n_0(x) = n_b + n_c\, x / L_n \ ,$$

$$(2) \qquad T(x) = T_0 \,(1 + x / L_T) \ ,$$

where n_b is the boundary density, and n_c the cut-off density (the density at which the plasma frequency equals the frequency of the wave). A vacuum gap, denoted as $x_{vac} \leq 2$ mm in the computations, may be present between the grill mouth and the plasma boundary. In the presence of the LH power, the density $n_0(x)$ in eq. (1) is modified according to the following formula /4/:

$$(3) \qquad n(x,z) = n_0\, e^{-\delta(x,z)}$$

with

$$(4) \qquad \delta = \varepsilon_0 \,|E_z|^2 / 4\, n_c\, T \ ,$$

ε_0 being the permittivity of the vacuum. Note that in the z-direction the density is modified only where $E_z \neq 0$. To account for the experimentally observed saturation of the reflection coefficient R with the LH power, an increase of the temperature with power has to be considered. We assume a simple dependence of T on power of the following form:

$$(5) \qquad T = T_0\,(1 + g)\,(1 + x / L_T),$$

where g depends on the Poynting flux S,

$$(6) \qquad g = (S / S_0)^2,$$

and S_0 is some constant.

Since we consider a very long grill launching a very narrow spectrum of waves, it is sufficient to treat only waves with one kz, or one N||. Higher spatial harmonics are neglected /4/. The ansatz for the electric fields is thus

$$(7) \qquad E_z(x,z) = E_1^{(+)}(x)\, \exp(ik_z z) + E_1^{(-)}(x)\, \exp(-ik_z z).$$

The basic equations are then /4/

$$(8) \qquad \frac{d^2E_1^{(\pm)}}{dx^2} + (k_0^2 - k_z^2)E_1^{(\pm)} = \frac{n_0(x)}{\lambda n_c}(k_0^2 - k_z^2)\int_0^{\lambda} \exp(\mp ik_z z - \delta(x,z))E_z(x,z)dz,$$

where $\lambda = 2\pi / k_z$, $k_0 = \omega / c$. These equations for $E_1^{(+)}$ and $E_1^{(-)}$ are solved numerically with boundary conditions chosen deep enough inside the plasma, where ponderomotive force effects are negligible /4,6/. The RF electromagnetic fields computed this way yield the values of the wave reflection coefficient $R_w(z)$ at the grill mouth. The power reflection coefficient, averaged over z, is then

$$(9) \qquad R = \int_0^{\lambda} S(z)\frac{|R_w^2(z)|}{1-|R_w^2(z)|}dz \left(\int_0^{\lambda} \frac{S(z)}{1-|R_w^2(z)|}dz\right)^{-1},$$

where S (z) is the x-component of the Poynting vector of the LH waves transmitted into the plasma.

3. The nonlinear reflection coefficient R

The computed power-dependent reflection coefficients are presented in figs. 3 to 11. In keeping with ASDEX experimental data /3/, the following values of the input parameters were chosen : $T_0 = 5 - 7.5$ eV, $L_n = 0.1 - 0.6$ cm, $L_T = 1 - 3$ cm, $n_b/n_c = 2 - 8$, $k_0 = 51.31$ m^{-1} (f = 2.45 GHz). The value x_{vac} of the vacuum gap between the grill and the plasma boundary was greater than zero only in fig. 11, $x_{vac} \leq 2$ mm. To approximate the measured values of the reflection coefficient R, we made S_0 correspond to the power density flux 1 - 2 kW/cm^2. In the ASDEX experiments the power density flux of the LH wave has been varied from 0 to 4 kW/cm^2.

In order to check our results against the linear coupling theory /9,10,11/, we show in figs. 3 the reflection coefficient at low LH power, i.e. S = 0, as a function of the edge density n_b. We see that R shows a minimum in the case $N_{||} = 2$ at $n_b/n_c \approx 4$, while for $N_{||} = 3$ and $N_{||} = 4$ this minimum is at a value of

n_b/n_c higher than the highest one used in our computations. This agrees well with linear coupling theory - if higher-order modes are neglected and the waveguide walls are taken very thin - which predicts this minimum of R at edge densities of $n_b = n_c N_{||}^2$ /10/.

Next we investigate the effect of the ponderomotive force alone, neglecting any possible heating of the plasma in front of the grill by the LH wave, i.e. we take g = 0 in eq (5). In figs. 4 and 5 we show with dashed lines results corresponding to different edge density and temperature profiles. In fig. 4 we have a flat density gradient L_n = 0.3 cm and a low temperature T_0 = 5eV with a flat gradient L_T = 3 cm. In this case the electron pressure is low and only slowly rises with x. For $n_b/n_c \leq 4$ and S = 0 we are on the left side of the minimum in R for all cases of $N_{||}$ computed (fig. 3), and thus a decreasing edge density due to the ponderomotive force leads to an increase of R with the power density S to values approaching 1. In fig. 4c this is not the case for $N_{||}$ = 2. Here we are on the right side of the minimum in R (fig. 3) and the decreasing edge density leads to a minimum of R as a function of S.

Similar behaviour is found in the dashed lines in fig. 5, where we have L_n = 0.1 cm, T_0 = 7.5 eV and L_T = 1cm, i.e. higher edge pressure with a steeper profile.The ponderomotive force in this case leads to a much weaker decrease in the edge density with a correspondingly slower variation of R with S. Nevertheless R increases with S and finally approaches 1.

The variation of R with S is quite different if we allow the edge plasma to get heated with increasing transmitted power flux S, i.e. if we take $g \neq 0$. This is shown in figs. 4 and 5 in the solid lines. Particularly in fig. 5, where from the outset we already have a higher electron pressure than in fig. 4, we see that R initially increases but saturates at high power fluxes owing to the concomitant rise in electron pressure. The growth of R with S and its saturation level are thus weaker in fig. 5 than in fig. 4.

The extent to which the edge density is modified by the ponderomotive force can be seen in fig. 6, where the profiles of n (x, z) are shown for the parameters of figs. 4b and 5b. The long dashed lines denote the unperturbed density profile, the short dashed lines the perturbed density if heating is neglected, g = 0, and the solid lines the perturbed density if heating is taken into account, $g \neq 0$. The density is seen to be modified only at the very edge in the range of a few millimeters in front of the grill and that the modification is

much less in the case of the higher electron pressure (fig. 6b). It is seen how the heating prevents a strong decrease of the edge density.

The dependence of the growth of R with S upon the density gradient is shown in fig. 7. Here, too, we see that in the case of the steeper gradient, $L_n = 0.1$ cm, the growth of R with S is weakest. Similarly, if we vary the electron temperature and its gradient are varied as in fig. 8, we get in the case of the lower pressure, $T_0 = 5$ eV and $L_T = 3$ cm, a much stronger effect of the ponderomotive force than in the case of higher pressure, $T_0 = 7.5$ eV and $L_T = 1$ cm.

In fig. 9 we examine the influence of the heating on the growth of R with S. Stronger heating, as in the case $S_0 = 1$ kW/cm^2, leads to a weaker increase of R with S and to a lower saturated level of R.

The dependence of the reflection coefficient R on the power S is stronger for higher $N_{||}$, as shown in fig. 10. The reason is that for the same power the wave electric field and hence also the ponderomotive forces are higher for higher $N_{||}$. Obviously, to obtain a closer fit to the experiment, the heating of the plasma by the wave (which is represented by the function g) should also depend on the value of $N_{||}$. To obtain better agreement with the experimen-tal data, this heating of the plasma by the wave just in front of the grill should be stronger for higher $N_{||}$.

We have also studied the influence of a vacuum gap between the grill and the plasma in order to model the case of protruding graphite tiles in the experiment. The results are shown in fig. 11. Already at low power such a vacuum gap has a considerable influence on the coupling, and the reflection coefficient increases quite strongly. With increasing power we also obtain a growing R with final saturation, although the relative growth is less in the case of the wider vacuum gaps.

All computations in figs. 3 to 11 were done for a wave propagating in the z-direction, the directivity D being high, $E_1^{(-)} \approx 0$. The directivity D is defined as $D = P^{(+)} / P^{(-)}$, where $P^{(+)}$ and $P^{(-)}$ are the powers connected with $E_1^{(+)}$ and $E_1^{(-)}$ (see eq. (7)), respectively. The dependence of R on D is plotted in fig. 12 for various S and $N_{||}$. For S ---> 0, R does not depend on D for any $N_{||}$. For higher $N_{||}$, the dependence of R on D is stronger since the ponderomotive forces are stronger for the same S in this case. The reason for such a dependence of R on D for $S \neq 0$ is the modulation (in the z-direction) of the plasma density by the ponderomotive forces of the standing wave.

4. Conclusion

We think that the cause of the variation of R with power is the variation of edge plasma parameters due to the ponderomotive forces. Electron heating in the edge region due to the transmitted power prevents the reflection coefficient from rising continuously; rather it leads to saturation as observed. However, our rough model of the grill and the edge plasma cannot be expected to give an exact fit to the experiment. Our computations indicate the importance of the thin plasma layer just in front of the grill on the coupling. In future large devices, local control of the plasma parameters in this region will be necessary /2/.

This work was initiated during a one-month stay of one of the authors (V.P.) at Garching in June/July 1989 and was continued during his second stay there in April/May 1990. He wishes to thank IPP Garching for the possibility of working there and for the kind hospitality accorded to him. . Both authors are grateful to Dr. F. Söldner, Dr. A. Tuccillo and the Lower Hybrid Group of IPP for discussions and for experimental data, and to Dr. M. Brambilla for his very kind help with the computer software.

The 2.45 GHz lower hybrid experiment on ASDEX was conducted in cooperation between IPP - Garching, ENEA - Frascati and PPPL - Princeton.

References

/ 1 / Leuterer F. et al., 16th EPS Conf. on Controlled Fusion and Plasma Physics, Venice 1989, Europhysics Conference Abstracts Vol. 13B, IV, 1287, (1989)

Leuterer F. et al., 8th Top. Conf. Radio Frequency Power in Plasmas, Irvine, California 1989, American Inst. of Physics Conf. Proc. Vol. 190, 95, (1989)

/ 2 / Leuterer F. et al., 17th EPS Conf. on Controlled Fusion and Plasma Physics, Amsterdam 1990, Europhysics Conference Abstracts Vol. 14B, III, 1287, (1990)

/ 3 / Schubert R. et al.,17th EPS Conf. on Controlled Fusion and Plasma Physics, Amsterdam 1990, Europhysics Conference Abstracts Vol. 14B, IV, 1525, (1990)

Tsois N. et al., 16th EPS Conf. on Controlled Fusion and Plasma Physics, Venice 1989, Europhysics Conference Abstracts Vol. 13B, III, 907, (1989)

El Shaer M., IPP Report III / 118 (1986), IPP Garching

/ 4 / Petrzilka V., Klima R., Pavlo P., J. Plasma Physics 30 (1983), 211; 11th EPS Conf. on Controlled Fusion and Plasma Physics, Aachen 1983, p. 315; Int. Conference on Plasma Physics, Lausanne 1984, p.220

/ 5 / Petrzilka V., Internal Report 9/89, IPP Prague

/ 6 / Fukuyama A., Morishita T., Furutani Y., Plasma Physics 22 (1980), 565

/ 7 / Teilhaber K., Nucl. Fusion 22 (1982), 363

/ 8 / Bermann R., et al., 8th IAEA Conf. Plasma Phys. and Contr. Nucl. Fusion Res., Brussels 1980, p. 493

/ 9 / Brambilla M., Nucl. Fusion 16 (1976), 47

/ 10 / Stevens J., et al., Nucl. Fusion 21 (1981), 1259

/ 11 / Moreau D., Report EUR-CEA-FC-1199 (1983)

Figures

Fig. 1 Average reflection coefficient R of the upper grill as a function of incident RF-power into the upper grill in the ASDEX lower hybrid experiment at 2.45 GHz . Grill with protruding protection tiles.
$B_t = 2.8$ T, $I_p = 420$ kA, $n_e = 1.35\ 10^{13}cm^{-3}$, $R_p = 168$ cm,
$R_g = 212.5$ cm

Fig. 2 Same as fig. 1, but grill with nonprotruding protection tiles

Fig. 3 Linear reflection coefficient R as a function of the edge density n_e.
$S = 0$.
a) $L_n = 0.3$ cm b) $L_n = 0.1$ cm

Fig. 4 Nonlinear reflection coefficient R as a function of the transmitted RF-power density S. Dashed lines : without heating of the edge plasma, $g = 0$.
Solid lines : with heating of the edge plasma, $g \neq 0$.
a) $n_b/n_c = 2$ b) $n_b/n_c = 4$ c) $n_b/n_c = 8$.
Other parameters :
$L_n = 0.3$ cm, $T_0 = 5$ eV, $L_T = 3$ cm, $S_0 = 2$ kW/cm^2, $x_{vac} = 0$.

Fig. 5 Same as Fig 4, but
a) $n_b/n_c = 2$ b) $n_b/n_c = 4$ c) $n_b/n_c = 6$.
Other parameters :
$L_n = 0.1$ cm, $T_0 = 7.5$ eV, $L_T = 1$ cm, $S_0 = 2$ kW/cm^2, $x_{vac} = 0$.

Fig. 6 Profiles of the edge density for the parameters of a) fig. 4b and b) fig. 5b
with $S = 4$ kW/cm^2, $N_{||} = 4$.
Long-dashed lines : unperturbed density
Short-dashed lines : without heating, $g = 0$
Solid lines : with heating, $g \neq 0$.

Fig. 7 Same as Fig. 4, but
a) $L_n = 0.1$ cm b) $L_n = 0.3$ cm c) $L_n = 0.6$ cm.
Other parameters :
$n_b/n_c = 4$, $T_0 = 7.5$ eV, $L_T = 1$ cm, $S_0 = 2$ kW/cm^2, $x_{vac} = 0$.

Fig. 8 Same as Fig. 4, but
a) $T_0 = 5$ eV, $L_T = 3$ cm b) $T_0 = 7.5$ eV, $L_T = 1$ cm.
Other parameters :
$n_b/n_c = 4$, $L_n = 0.3$ cm, $S_0 = 2$ kW/cm^2, $x_{vac} = 0$.

Fig. 9 Same as Fig. 4, but
a) $S_0 = 1$ kW/cm^2 b) $S_0 = 2$ kW/cm^2.
Other parameters :
$n_b/n_c = 4$, $L_n = 0.3$ cm, $T_0 = 7.5$ eV, $L_T = 1$ cm, $x_{vac} = 0$.

Fig. 10 Variation of reflection coefficient R with $N_{||}$ at different power densities.
Other parameters :
$n_b/n_c = 4$, $L_n = 0.3$ cm, $T_0 = 5$ eV, $L_T = 3$ cm, $S_0 = 2$ kW/cm^2, $x_{vac} = 0$.

Fig. 11 Same as Fig. 4, but
a) $x_{vac} = 0$ b) $x_{vac} = 1$ mm c) $x_{vac} = 2$ mm.
Other parameters :
$n_b/n_c = 4$, $L_n = 0.1$ cm, $T_0 = 7.5$ eV, $L_T = 1$ cm, $S_0 = 2$ kW/cm^2.

Fig. 12 Variation of the reflection coefficient R with directivity D at different $N_{||}$ and power densities.
Other parameters :
$n_b/n_c = 4$, $L_n = 0.3$ cm, $T_0 = 5$ eV, $L_T = 3$ cm, $S_0 = 2$ kW/cm^2, $x_{vac} = 0$.

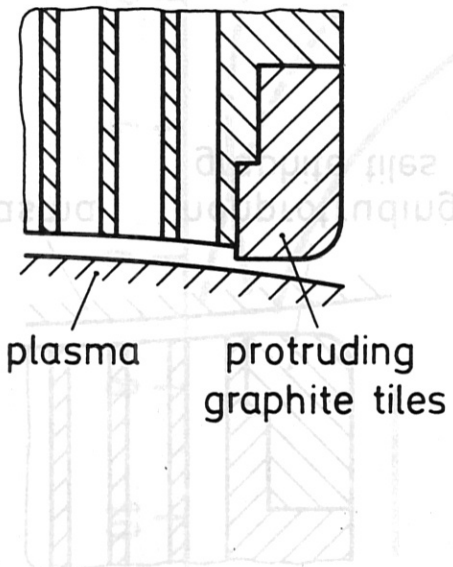
plasma
protruding
graphite tiles

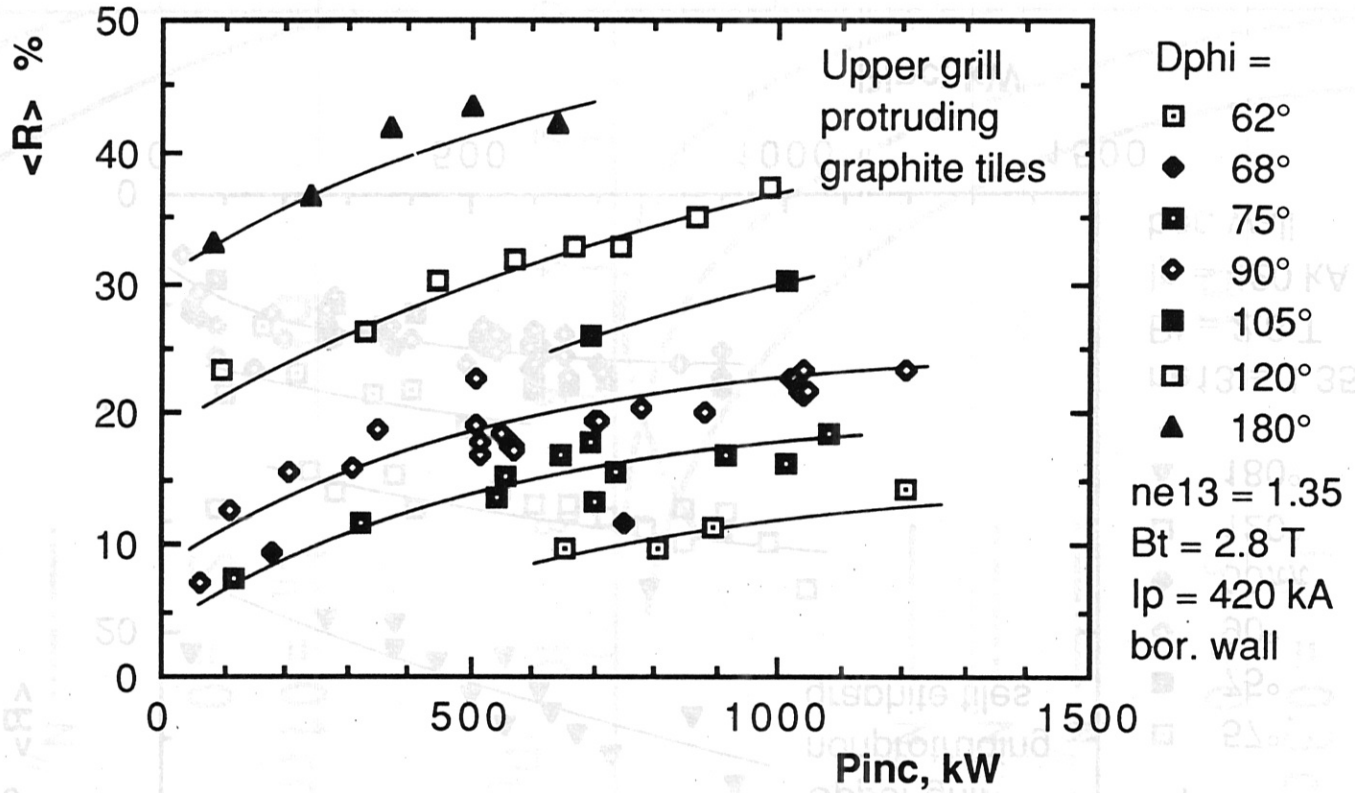
<R> %
50
40
30
20
10
0
0
500
1000
1500
Pinc, kW
Upper grill
protruding
graphite tiles
Dphi =
62°
68°
75°
90°
105°
120°
180°
ne13 = 1.35
Bt = 2.8 T
Ip = 420 kA
bor. wall

Fig.1

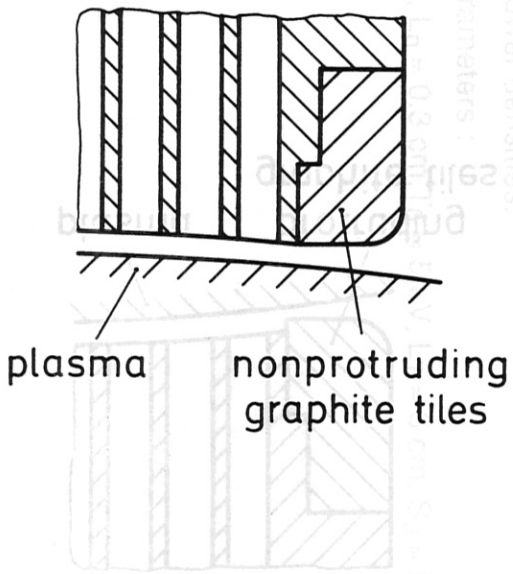
plasma
nonprotruding
graphite tiles

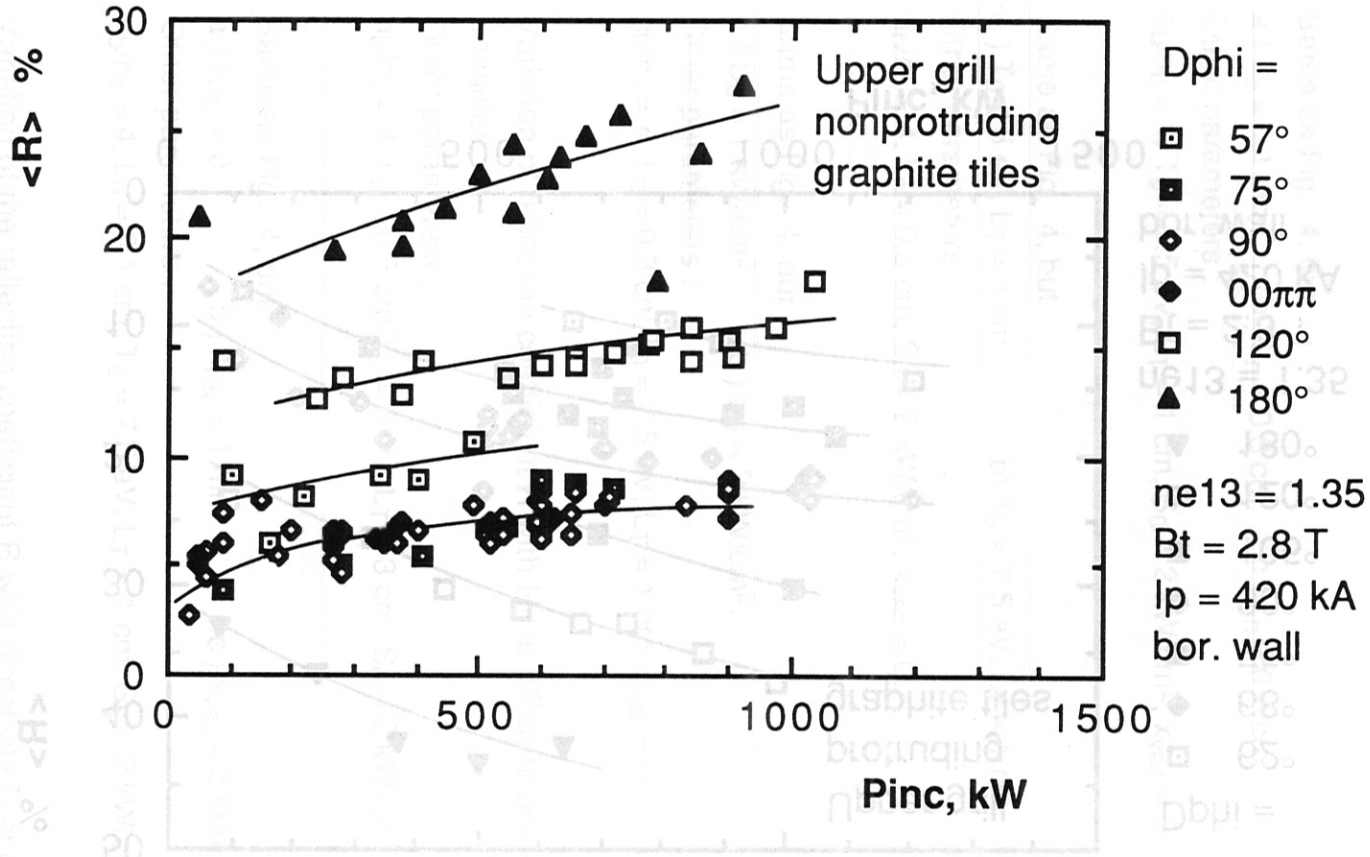
<R> %
30
20
10
0
0
500
1000
1500
Pinc, kW
Upper grill
nonprotruding
graphite tiles
Dphi =
57°
75°
90°
00ππ
120°
180°
ne13 = 1.35
Bt = 2.8 T
Ip = 420 kA
bor. wall

Fig. 2

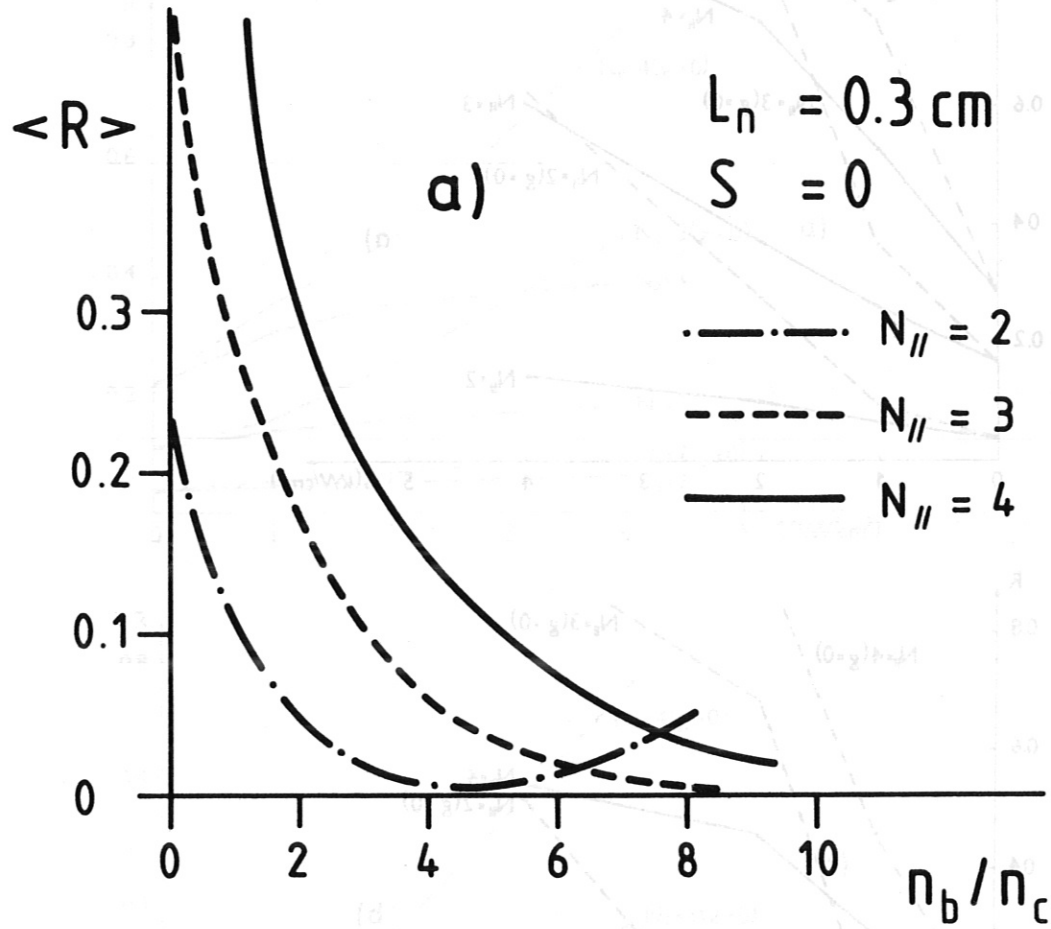
<R>
a)
L_n = 0.3 cm
S = 0
$N_{//}$ = 2
$N_{//}$ = 3
$N_{//}$ = 4
0.3
0.2
0.1
0
0
2
4
6
8
10
n_b / n_c

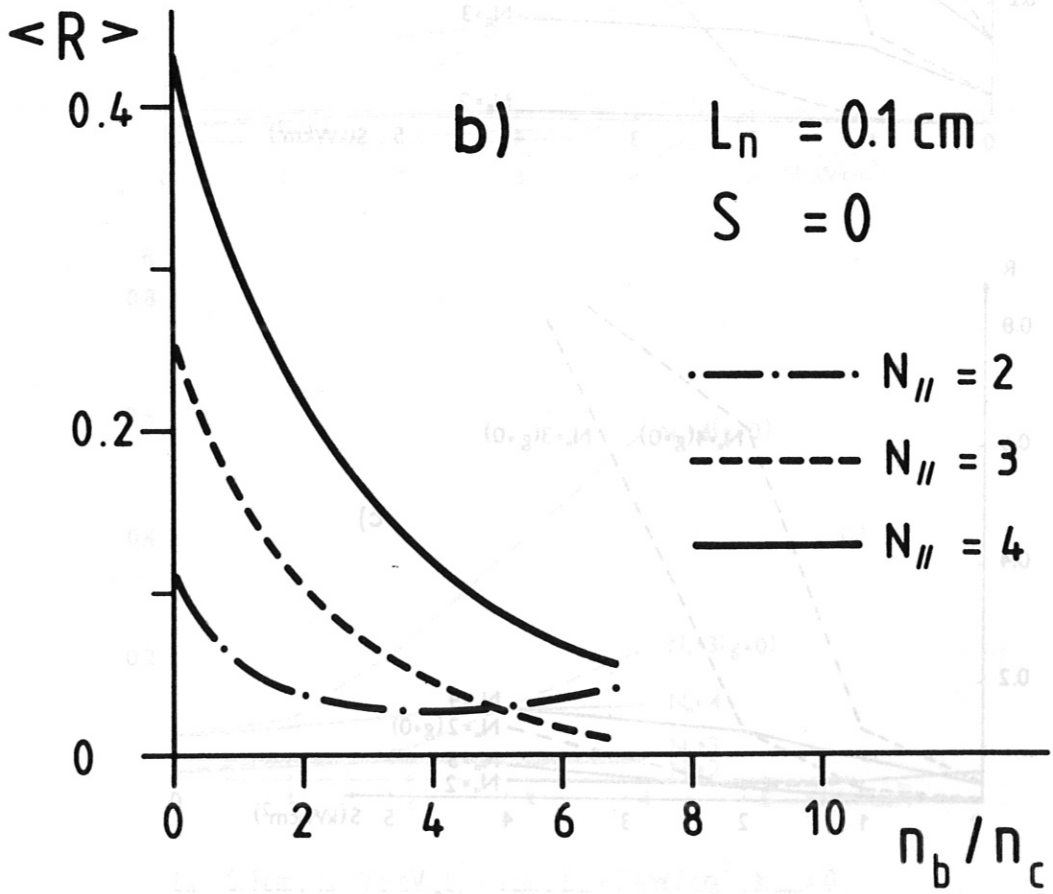
<R>
b)
L_n = 0.1 cm
S = 0
$N_{//}$ = 2
$N_{//}$ = 3
$N_{//}$ = 4
0.4
0.2
0
0
2
4
6
8
10
n_b / n_c

Fig. 3

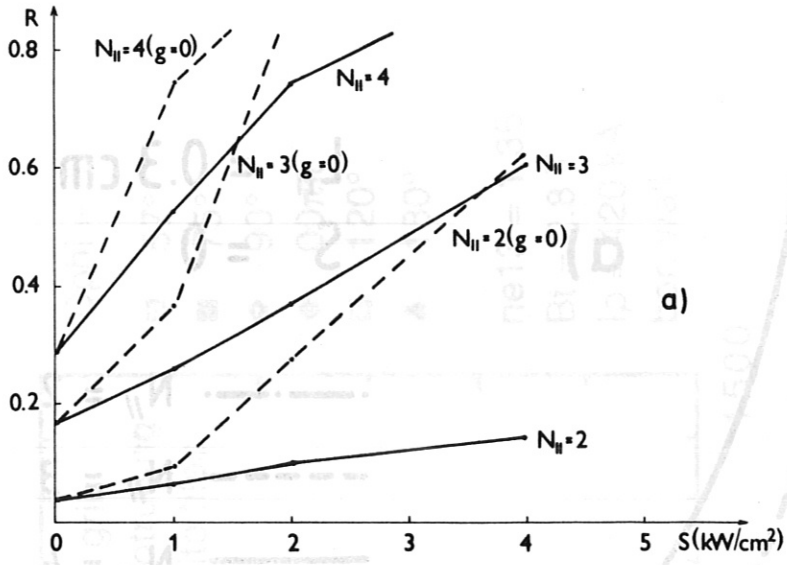

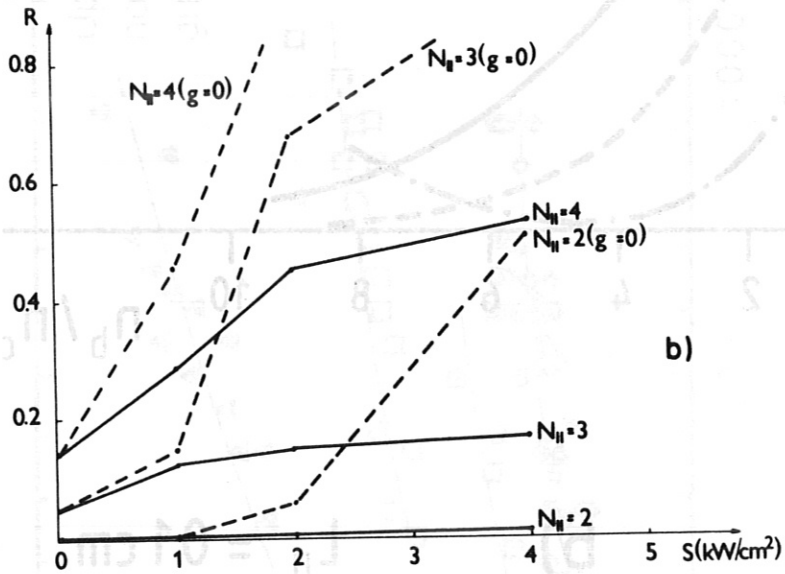

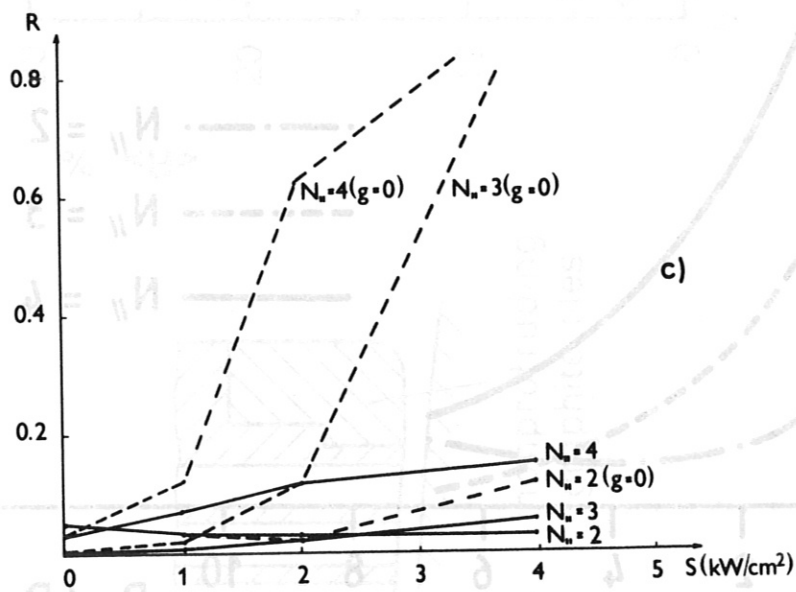

$L_n = 0.3\,cm$; $T_0 = 5\,eV$; $L_T = 3\,cm$; $E_0 = 2\,kW/cm^2$; $X_{vac} = 0$

Fig. 4

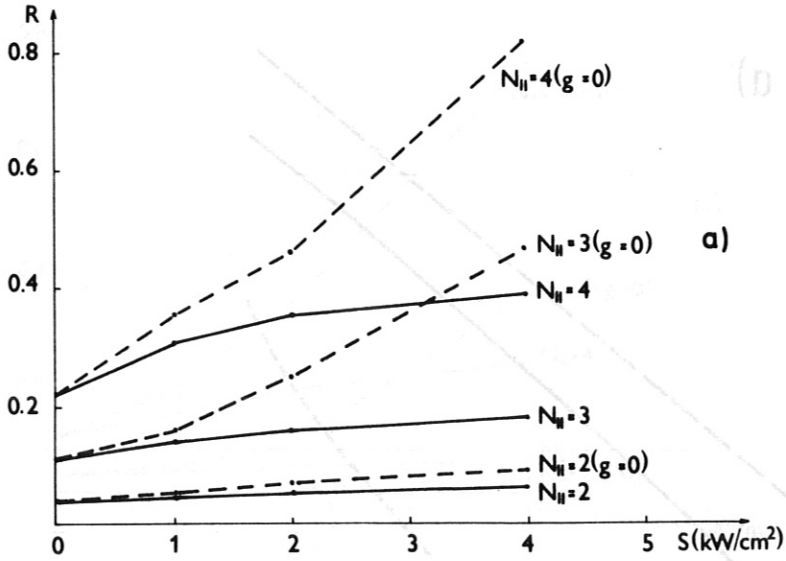

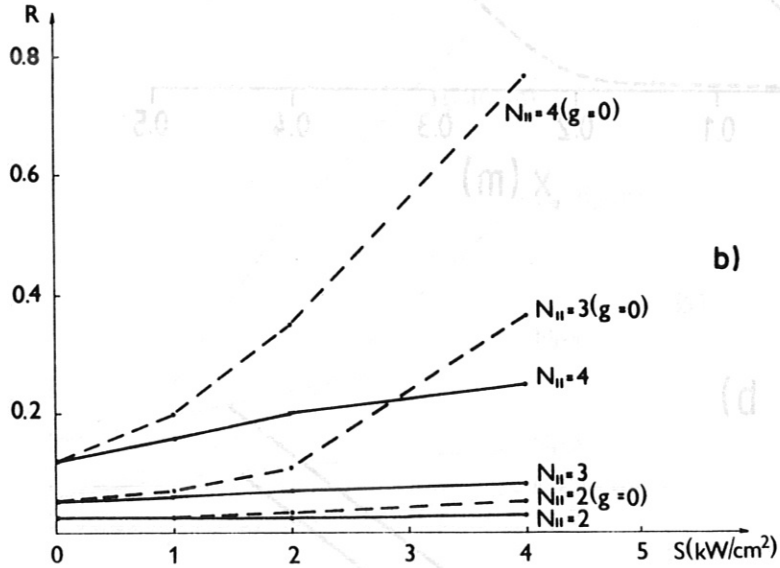

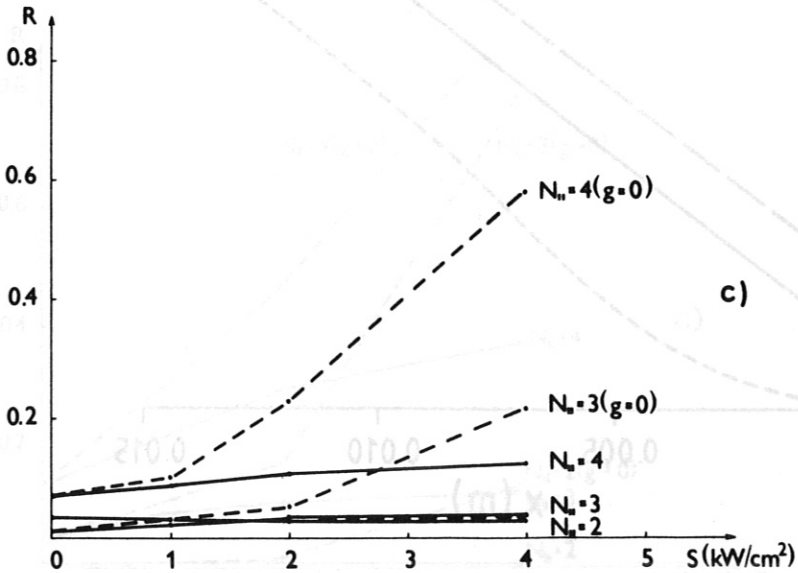

$L_n = 0.1\,cm$; $T_0 = 7.5\,eV$; $L_T = 1\,cm$; $E_0 = 2\,kW/cm^2$; $X_{vac} = 0$

Fig. 5

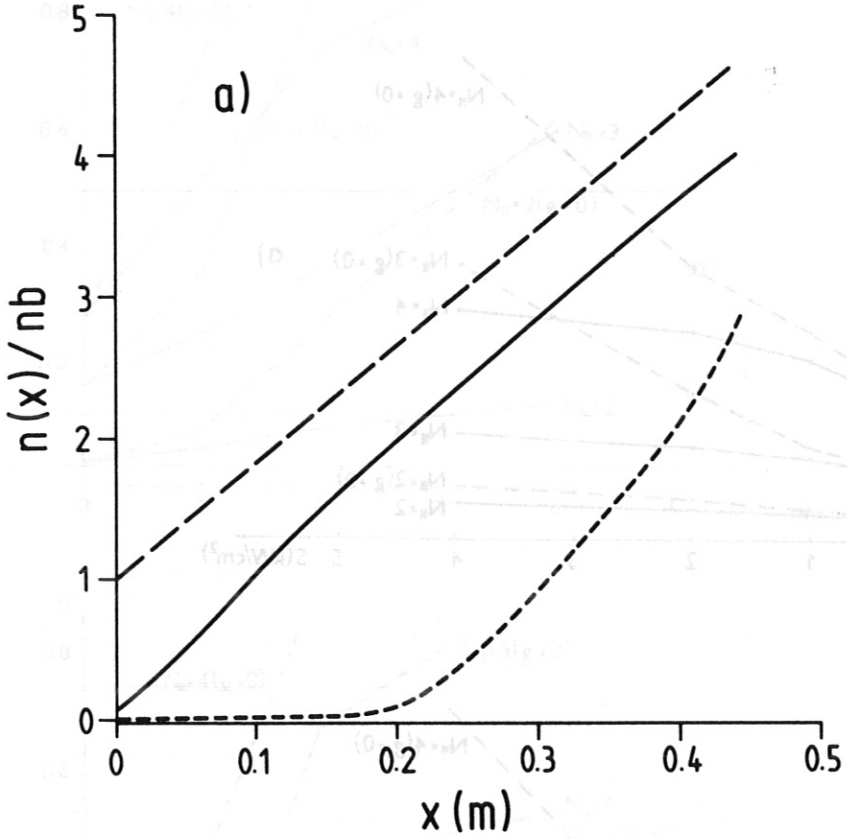

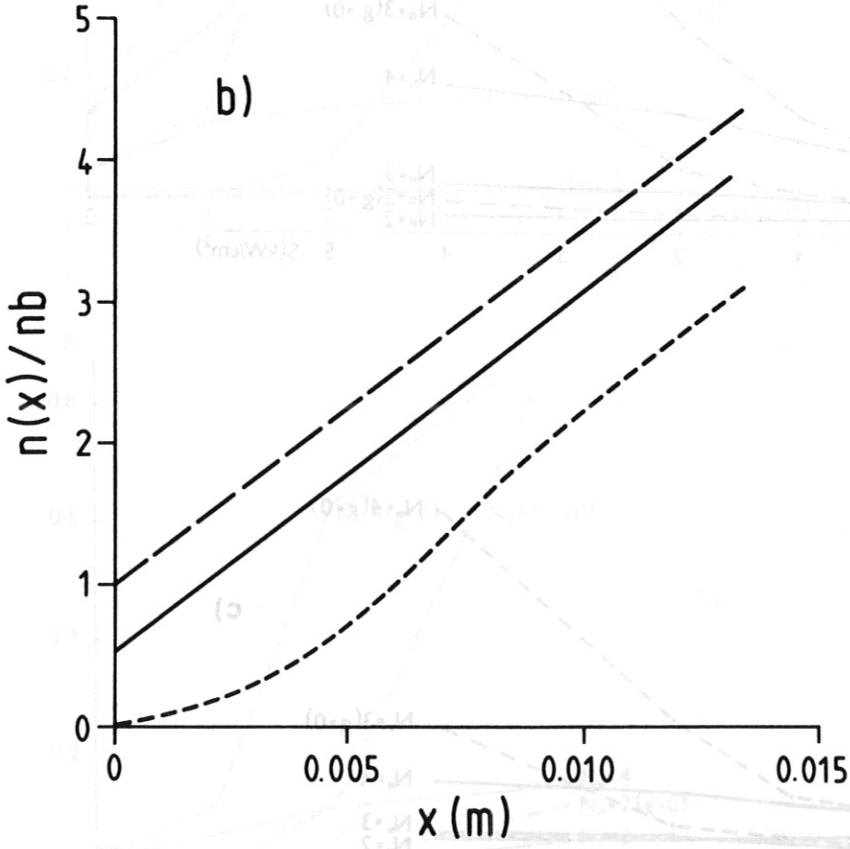

$n_b/n_c = 4$; $E_0 = 2\,kW/cm^2$; $X_{vac} = 0$

Fig. 6

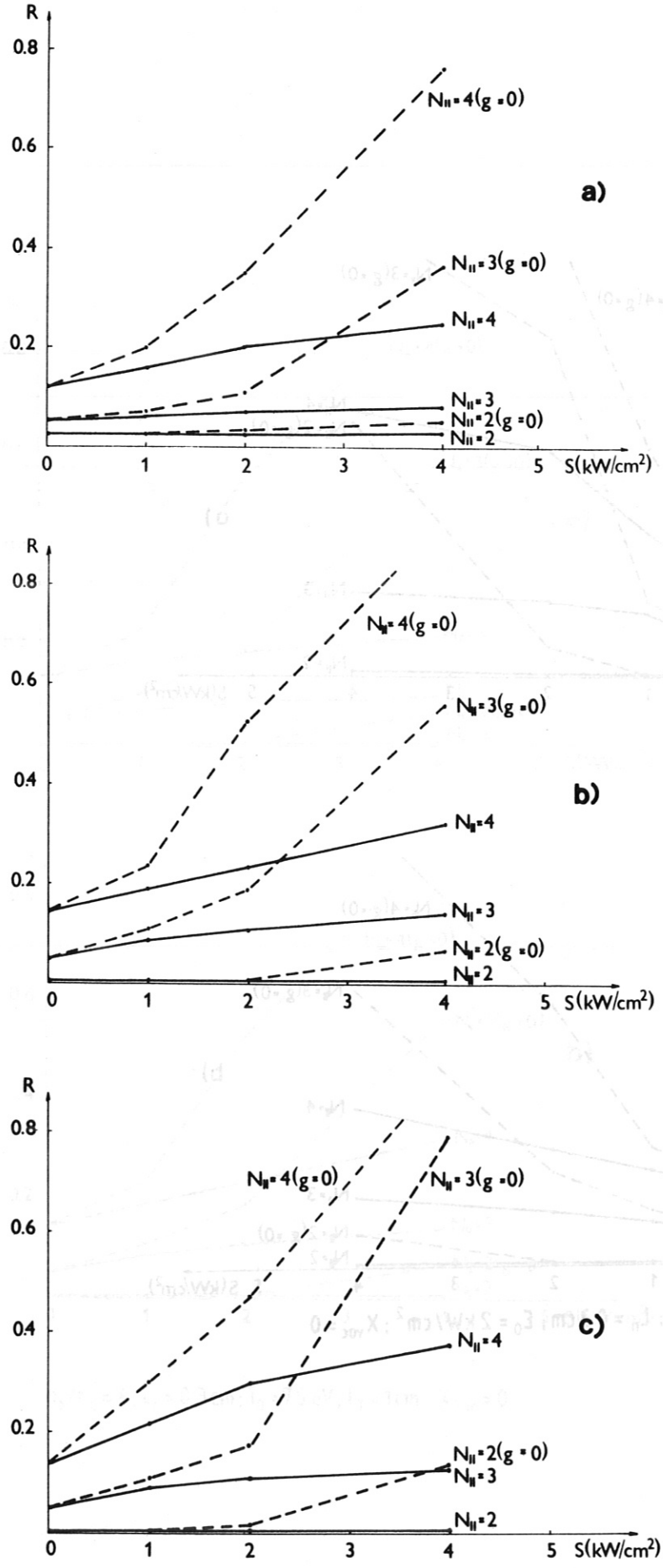

$n_b/n_c = 4$; $L_n =$ cm; $T_0 = 7.5$ eV; $L_T = 1$ cm; $E_0 = 2$ kW/cm^2; $X_{vac} = 0$

Fig. 7

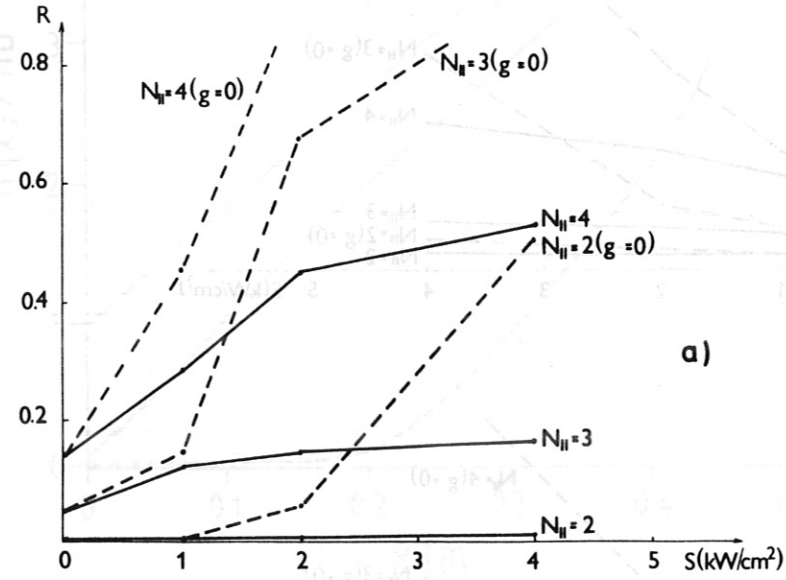

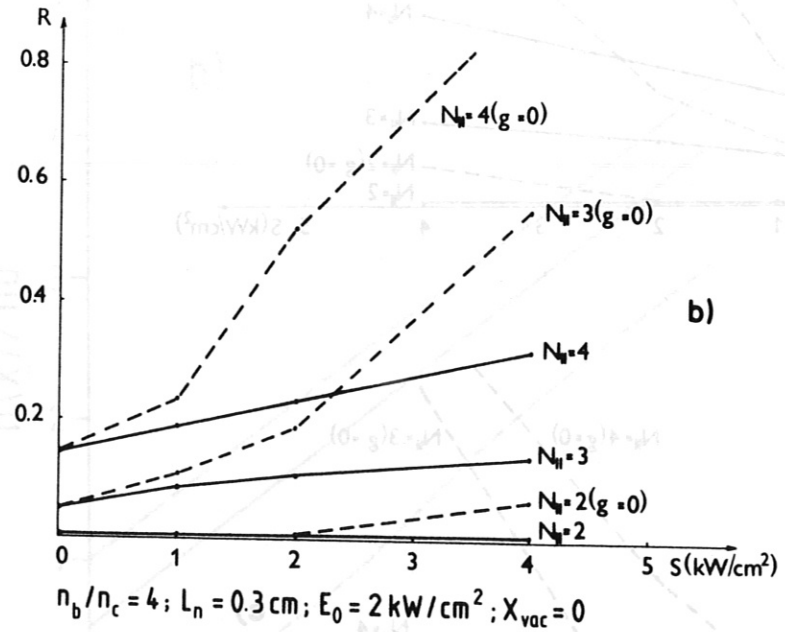

$n_b/n_c = 4$; $L_n = 0.3$ cm; $E_0 = 2$ kW/cm^2; $X_{vac} = 0$

Fig. 8

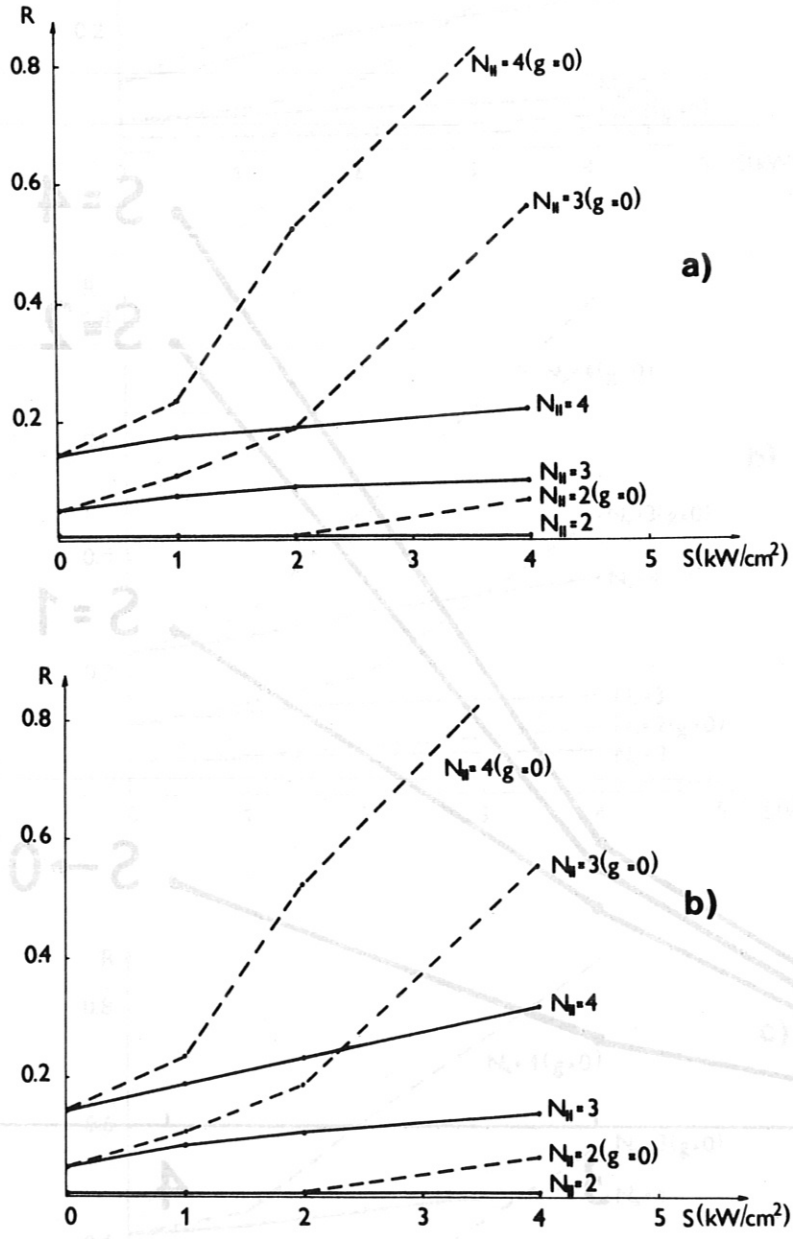

$n_b/n_c = 4$; $L_n = 0.3\,cm$; $T_0 = 7.5\,eV$; $L_T = 1\,cm$; $X_{vac} = 0$

Fig.9

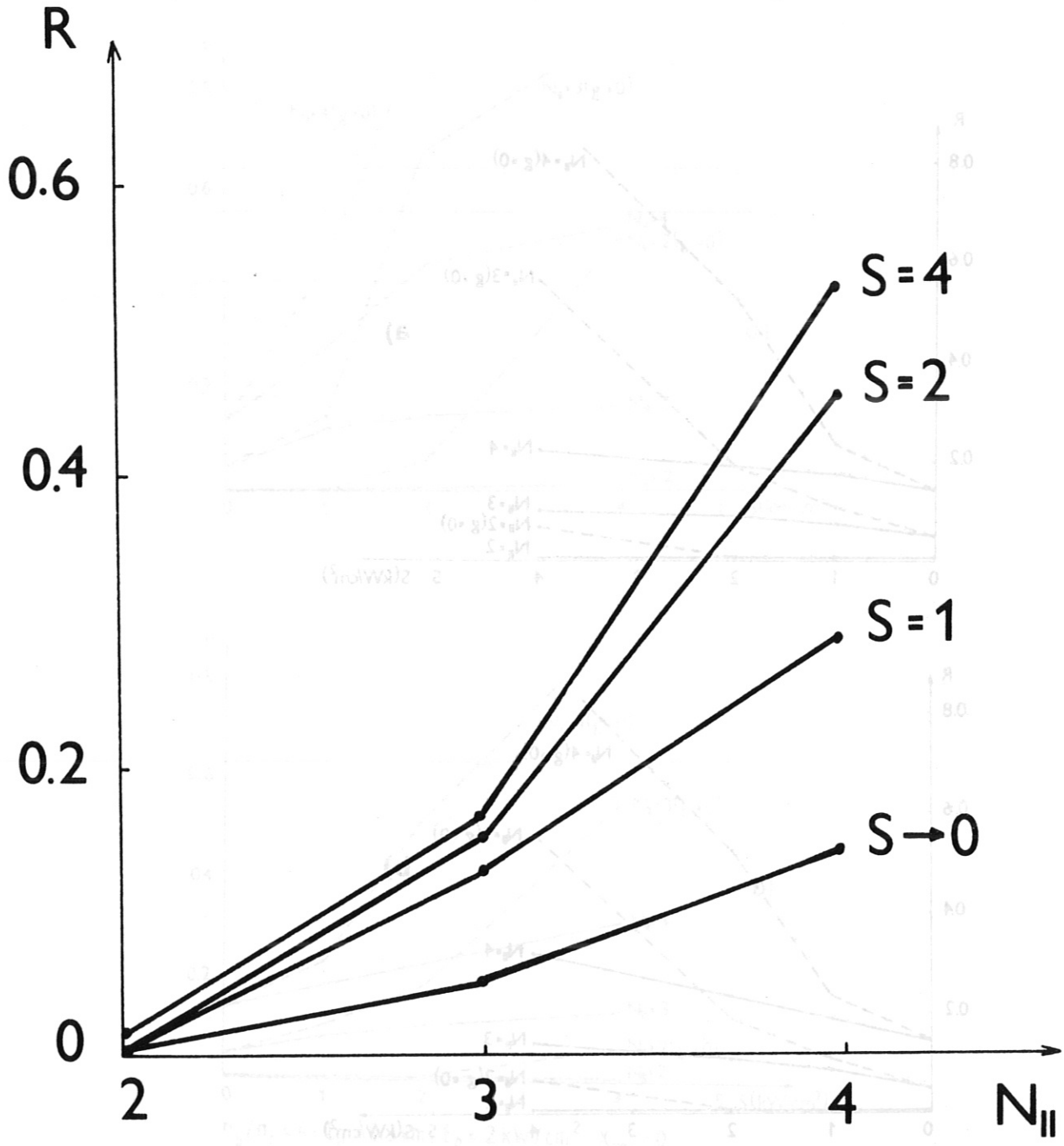

Fig. 10

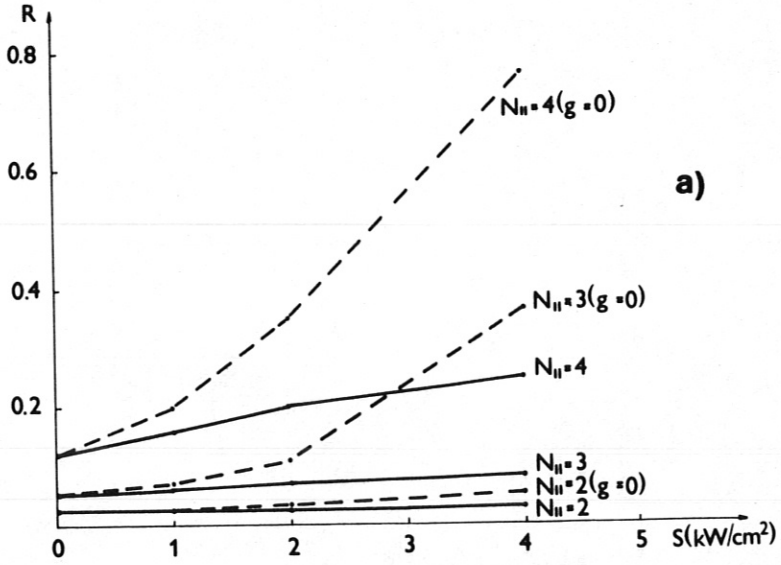

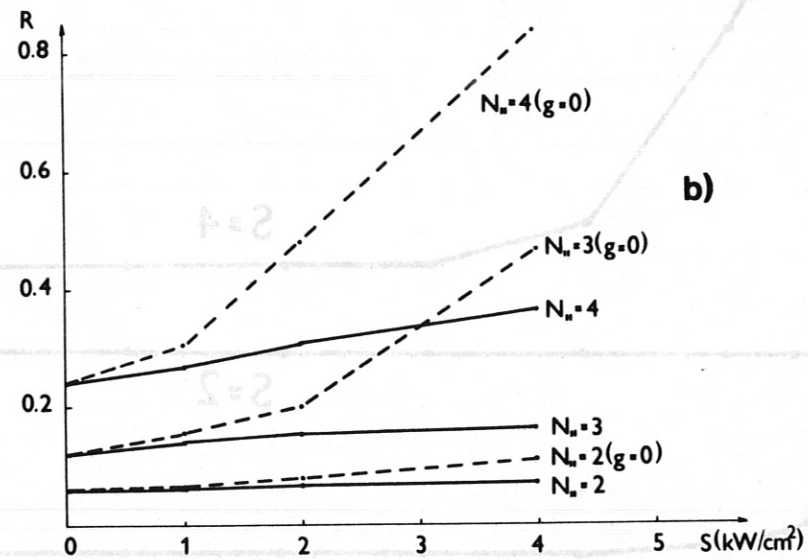

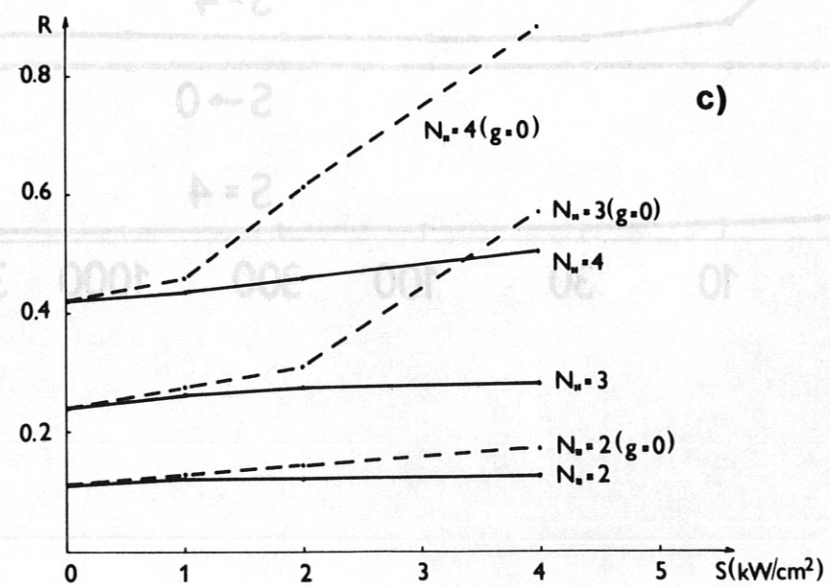

$n_b/n_c = 4$; $L_n = 0.1\,cm$; $T_0 = 7.5\,eV$; $L_T = 1\,cm$; $E_0 = 2\,kW/cm^2$

Fig. 11

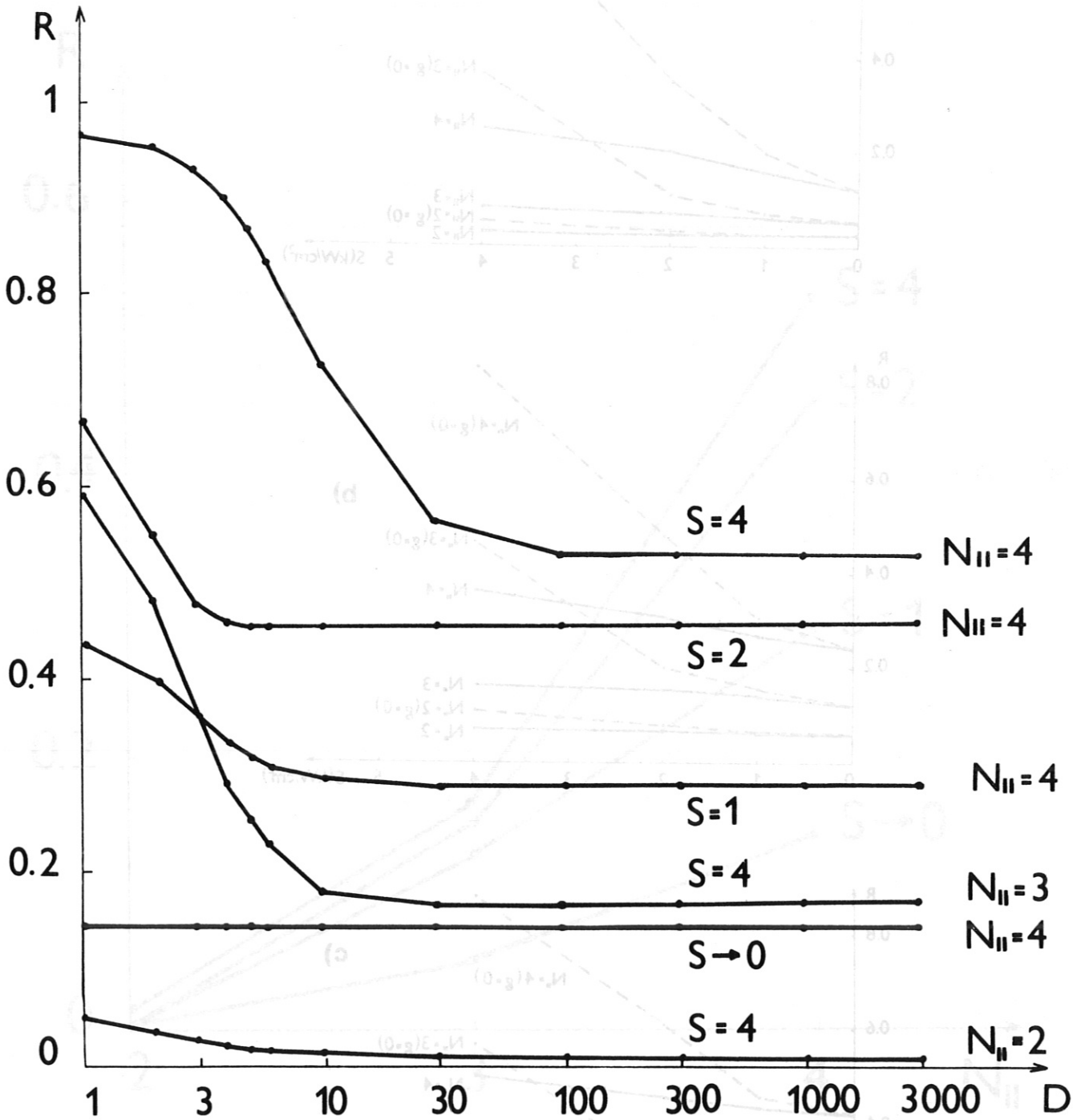
R
1
0.8
0.6
0.4
0.2
0
1
3
10
30
100
300
1000
3000
D
S=4
N_II=4
S=2
N_II=4
S=1
N_II=4
S=4
N_II=3
S→0
N_II=4
S=4
N_II=2

Fig. 12